Recrystallization of an AlMgSi Alloy after Different Modes of Hot Deformation

TANJA PETTERSEN and ERIK NES

Recrystallization of an AlMgSi alloy has been studied after deformation in torsion and plane strain compression. The main emphasis has been focused on describing the development of nuclei in shear deformed material, and a physically based model has been developed to predict the course of recrystallization in torsion. This model is based on and compared to a previously developed model by Vatne *et al.*[1–4] describing the recrystallization in plane strain compressed material. To test the model predictions, recrystallization experiments on plane strain compressed and torsionally deformed material have been carried out.

I. INTRODUCTION

THE microstructures of the deformed material, the deformed state, define the conditions for the subsequent recrystallization and annealing processes. Parameters such as the stored energy, the deformation texture, the network of high-angle and low-angle boundaries, and the particle distribution are all important inputs when the objective is to model the recrystallization mechanism.[5] Different deformation modes result in different microstructures and textures, and a model developed for one mode may not be directly transferable to a different mode of deformation.

The development of deformation microstructure as well as the recrystallized microstructure and texture in plane strain compressed material has been extensively treated in several previous investigations.[1–4,6–10] The present work does not aim at giving such a thorough investigation, and parts of this presentation will rely on previously obtained results. Deforming a material in plane strain compression is often found to result in a structure consisting of large elongated grains containing a network of cells and subgrains, and constituting a texture typically consisting of the β fiber in addition to small amounts of Cube subgrains. When annealing, the Cube texture is found to play a significant role, with the nucleation from Cube subgrains as one of the main nucleation mechanisms.[1–4] Grain boundaries have also been shown to play an important role in nucleation of random grains, in addition to large particles when present. A model containing these nucleation mechanisms has been demonstrated to give a satisfactory description of the recrystallization in a plane strain compressed AlMgMn alloy.[1–4] An important result is that the grain size decreases and the strength of Cube increases with increasing strain prior to annealing.

During industrial deformation processes such as rolling and extrusion, the deformation is often seen to be a combination of different deformation modes. The recrystallization process accordingly depends on the preceding deformation process, described by the deformation mode in addition to parameters such as strain, strain rate, and temperature. The objectives of the present investigation have been to provide knowledge about the development of microstructure and texture during recrystallization of material deformed at different deformation modes, and to investigate possible similarities.

TANJA PETTERSEN, Senior Engineer, is with R&D Materials Technology, Hydro Aluminium a.s., N-6601 Sunndalsøra, Norway. Contact e-mail: tanja.pettersen@hydro.com E. NES, Professor, is with the Department of Materials Technology, Norwegian University of Science and Technology, N-7491 Trondheim, Norway.

Manuscript submitted May 7, 2003.

II. EXPERIMENTAL METHODS

An AA6060 alloy (0.49 wt pct Mg, 0.42 wt pct Si, 0.20 wt pct Fe, and balance Al) was used for the experimental investigations. Deformation was carried out in plane strain compression and torsion at various combinations of strain rates and temperature and to various strains. It is convenient, in this context, to use the temperature-compensated strain rate (Zener–Hollomon parameter);

$$Z = \dot{\varepsilon} \exp(U/RT) \quad [1]$$

where $\dot{\varepsilon}$ is the strain rate, U is an activation energy, R is the gas constant, and T is the temperature. Throughout this work, an activation energy of 156 kJ/mol has been used.

After the deformation, the specimens were annealed to obtain a partly or fully recrystallized microstructure. The annealing treatment was carried out by direct immersion of the test pieces into a salt bath, keeping the samples at this temperature for various times and followed by water quenching. Prior to deformation, the material deformed in torsion was homogenized at 580 °C and then quenched in water or slowly cooled, while the material deformed in plane strain compression was homogenised at 580 °C and cooled at a rate of ~200 °C/h.

A. *Processing of the Material*

Hot torsion tests were carried out to provide material for the annealing experiments. For details on the torsion experiments, see Reference 11. Plane strain compression (PSC) experiments were carried out on a Gleeble 3500 machine (DSI, Dynamic Systems Inc. Poestenkill, NY) with PSC-sample geometry of $40 \times 25 \times 10\ mm^3$. The unaltered results from the Gleeble machine give stress-strain curves with continuously increasing flow stress due to friction. The Terrapin algorithm developed at the University of Sheffield was applied to correct the results for friction; for a more detailed description on the Terrapin algorithm, see Silk and Winden.[12]

B. *Microstructural Characterization and Measurement of Texture*

Measurements of global textures were carried out on a Siemens (Siemens AG, Karlsruhe, Germany) D5000 X-ray diffractometer. For the torsion textures, experimental details are given in Pettersen and Nes.[13] When representing textures from the torsionally deformed specimens by Miller indices, the $\{hkl\}$ direction is parallel to the z direction and $<uvw>$ is parallel to the θ direction, that is, the representation is in the form $\{z\}<\theta>$ (for a detailed description of the texture evolution in torsion, see Reference 13). All the PSC specimens were cut in the longitudinal transverse section, that is, with the transverse direction normal to the plane of the specimen. When representing textures from the PSC samples by Miller indices ($\{hkl\}<uvw>$), the $\{hkl\}$ direction is parallel to the normal of the sheet and the $<uvw>$ direction is parallel to the rolling direction. This makes the representation of the PSC textures comparable to the representation of the torsion textures.

Optical microscopy and scanning electron microscopy along with a electron back scatter diffraction (EBSD) unit were used to investigate the as-deformed, the partly recrystallized and the fully recrystallized material. The torsion specimens were examined in the $z\theta$ plane, while the plane strain compressed material was examined in the rolling direction–normal direction (RD-ND) plane. When studying torsion samples, care was taken to keep the distance from the center of the specimen to the plane of study the same in all specimens. Optical microscopy was mainly used for measurements of recrystallized grain size in the fully recrystallized material. The grain size was measured by a linear intercept method, and the mean intercept length is given by

$$D = (D_\theta^2 \cdot D_z)^{1/3} \quad [2]$$

for the torsion specimens. For the plane strain compressed specimens, θ is replaced by the RD, while z is replaced by the ND.

III. RESULTS

The as-cast starting material consisted of a coarse, equiaxed grain structure, and the average mean intercept length was measured to be 100 μm. The texture of the starting material has previously been reported, and a close to random texture with a Cube volume fraction of 5 pct. For further details, see Reference 13.

A. Plane Strain Compression

Specimens were deformed at four different Zener–Hollomon parameters ($Z = 2{\cdot}10^8$ s^{-1}, $2{\cdot}10^{10}$ s^{-1}, $6{\cdot}10^{11}$ s^{-1}, and $1{\cdot}10^{12}$ s^{-1}; corresponding temperatures and strain rates are given in Table I) and to various strains. The deformation texture was measured using X-rays, and were found to reveal typical hot rolling textures, with components belonging to the α and β fibers. The Bs, S, Cu, and Goss components were seen to be relatively strong in all the as-deformed textures; in addition, clearly noticeable amounts of the Cube component were seen. The volume fractions of the various texture components have been calculated, and the results are listed in Table I. Of the components belonging to the α and β fibers, S and Bs seem to be the major components. This is especially the case at the higher strains. The volume fraction of Cube is, as expected, relatively small, ranging from about 3 pct to about 6 pct. That is, values that are all quite close to the average volume fraction expected in a randomly oriented aggregate of crystals, corresponding roughly to the Cube volume fraction in the initial, nondeformed state.

After deformation, the PSC samples were recrystallized, and the recrystallization texture and the recrystallized grain sizes were measured. The results from these measurements are listed in Table II. Unfortunately, the specimens deformed at lower Zener–Hollomon parameters were too coarse grained for X-ray analysis, so texture data for $Z < 6{\cdot}10^{11}$ s^{-1} are not available. The intensity of Cube is seen to increase with increasing prior strain. However, at the lowest strains, the intensity of the retained rolling texture components (Bs, S, and Goss) was seen to be stronger than the intensity of Cube. The recrystallized grain sizes are seen from the table to decrease with an increasing Zener–Hollomon parameter and increasing prior strain.

B. Torsion

A set of torsion experiments was carried out with Zener–Hollomon parameters ranging from $1.5{\cdot}10^8$ s^{-1} to $2{\cdot}10^{12}$ s^{-1}, and with strains ranging from 1 to 35. The temperature of deformation was kept above the solvus temperature to keep the hardening elements in solid solution during deformation. For a detailed description of these torsion experiments including the development of the stress-strain curve and the development of the deformation texture and microstructure, see Reference 13. In addition, a set of experiments was carried out on material slowly cooled after homogenisation, with Zener–Hollomon parameters ranging from $4{\cdot}10^{11}$ s^{-1} to $1{\cdot}10^{16}$ s^{-1}.

1. *Bs-oriented regions in the material deformed in torsion*

One of the common texture components resulting from cold rolling or plane strain deformation of fcc metals is brass,

Table I. The Volume Fraction of the Typical Rolling Texture Components for the Material Deformed in Plane Strain Compression

Z (s^{-1})	Temperature (°C)	Strain Rate (1/s)	Strain	S (Pct)	Bs (Pct)	Cu (Pct)	Goss (Pct)	Cube (Pct)
$2{\cdot}10^8$	520	0.01	0.9	—	—	—	—	—
$2{\cdot}10^{10}$	518	0.9	1.7	24	20	9	11	6
$6{\cdot}10^{11}$	482	10	0.4	20	15	9	9	4
$6{\cdot}10^{11}$	484	10	0.9	20	22	7	13	3
$6{\cdot}10^{11}$	484	10	1.7	23	24	7	14	4
$1{\cdot}10^{12}$	462	10	0.9	21	21	7	11	4

Table II. Volume Fraction of the Cube Component and Recrystallized Grain Size (Measured as Mean Intercept Lengths) in Various Plane Strain Compressed and Recrystallized Conditions

Z (s^{-1})	Strain	Cube (Pct)	Grain Size (μm)
$2 \cdot 10^{10}$	1.7	—	364
$6 \cdot 10^{11}$	0.4	7	124
$6 \cdot 10^{11}$	0.9	9	110
$6 \cdot 10^{11}$	1.7	17	87
$6 \cdot 10^{11}$	2.3	—	74
$1 \cdot 10^{12}$	0.9	10	95
$1 \cdot 10^{12}$	1.7	—	58

Bs ({011}<211>). As will be shown subsequently, this texture component also appears as a dominating recrystallization texture component in the present AA6060 alloy after deformation in torsion, and it will be referred to as Bs also in this context. Hence, a search for the Bs-oriented regions in the as-deformed (torsion) material was carried out in order to monitor potential nucleation sites. The appearance of the Bs-oriented regions was found to be strongly dependent on strain.

At small strains, two different types of Bs-oriented regions were found. The orientation image microscopy (OIM) map shown in Figure 1(a) shows an elongated band of the Bs orientation; in addition, small groups of subgrains of the Bs orientation not associated with bands were found. The lengths and widths of the bands were found to be close to what was expected from geometry. The areas adjacent to the Bs-oriented bands were characterized by orientation measurements and the results are displayed in Figure 2(a). It can be seen that a large fraction of the Bs-oriented bands are surrounded by regions of random orientation, which indicates that there are no preferred neighboring orientations.

At large strains, the Bs-oriented regions were solely present as single subgrains or small groups of subgrains (Figures 1(b) and (c)). The areas surrounding the subgrains were often found to be of the B^1 orientation, and a gradual orientation change from the B^1 orientation to the Bs orientation by rotation about a mutual <111>-axis was commonly observed. To obtain a quantitative measure of this phenomenon, the orientations of subgrains close to the Bs-oriented region were monitored, and the results are displayed in Figure 2(b). As can be seen from the figure, the great majority of the neighboring subgrains were of an orientation rotated an angle θ around the <111> axes from the B^1 orientation, or of the B^1 orientation. Just a small fraction of the surrounding subgrains were of the C or the random orientation. This indicates that the Bs regions have been formed by a rotation of the boundary region of the B^1-oriented bands. The fraction of the Bs regions surrounded by the C orientation decreases with strain, as the fraction of C-oriented bands decreases with strain. The regions of random orientation were seen to be similar to the regions of the Bs orientation; that is, the random oriented subgrains either formed small groups or single subgrains. The fraction of subgrains of random orientation, however, was found to decrease dramatically with strain from a strain of 5 to a strain of 25, compared to the fraction of subgrains of the Bs orientation, which was found to be approximately constant in the same strain range.

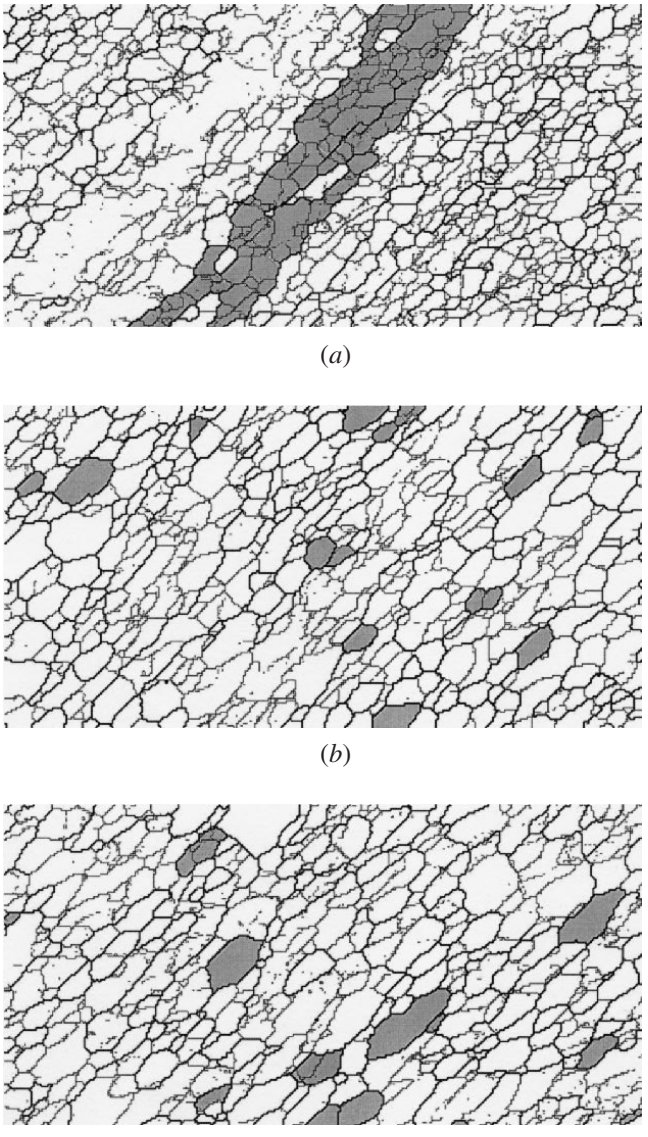

(*a*)

(*b*)

(*c*)

Fig. 1—OIM showing subgrains of the Bs orientation as shaded areas. The maps are from material deformed at $Z = 7 \cdot 10^{11}$/s, and to strains of (*a*) $\varepsilon = 1$, (*b*) $\varepsilon = 5$, and (*c*) $\varepsilon = 25$. A boundary is designated a high-angle boundary (heavy line) if the rotation angle is greater than 15 deg, and as a low-angle boundary (thin line) if the orientation difference lies below 15 and above 1.5.

2. *The partly recrystallized material*

In order to be able to investigate the course of the restoration processes in the hot torsion deformed material, the material was annealed to various stages of softening and then quenched. Using OIM, the orientations of new grains were recorded, and the results are shown in Table III. It can be seen that the number of new grains of the Bs-orientation increases with strain. This is in accordance with the increasing intensity of Bs in the fully recrystallized material. The Bs-oriented growing grains were found to be, on average, larger than the growing grains of other orientation. This was particularly the case at the highest strains, and at a strain of 25, the size difference was estimated to be about 1:5. The density of potential grains was found to increase with strain.

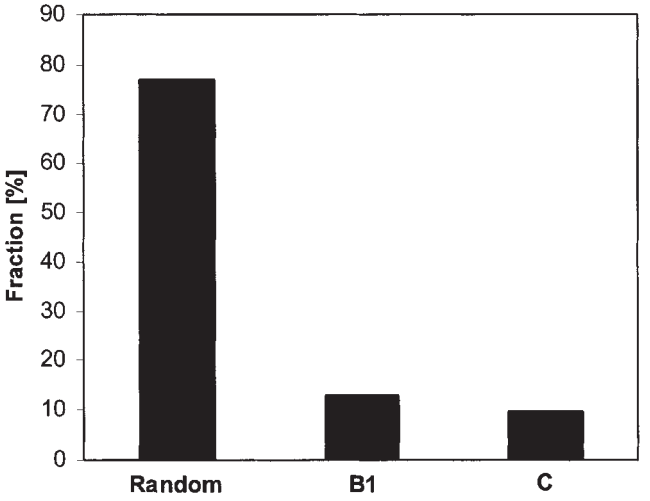

(*a*)

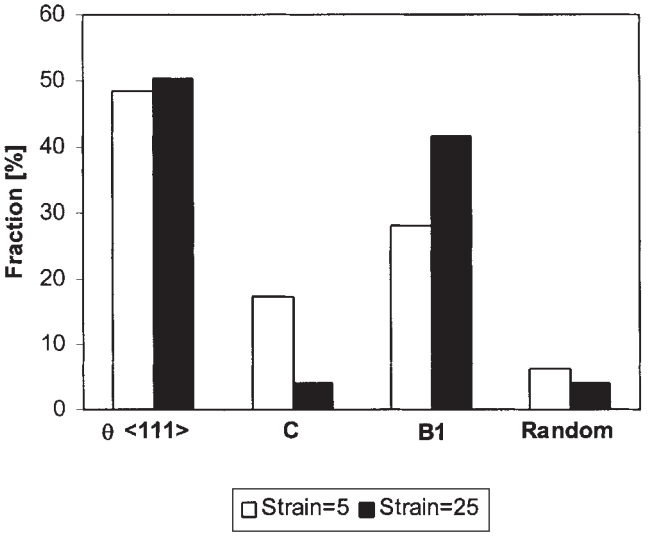

(*b*)

Fig. 2—Results from OIM. (*a*) Fraction of grains of various orientations surrounding the Bs-oriented bands. The measurement was carried out in the material deformed at $Z = 7 \cdot 10^{11}$/s deformed to a strain of 1. The values have been obtained by scanning about 1700 μm of the boundary area of the Bs-oriented bands. (*b*) Orientations of the regions surrounding the Bs-oriented subgrains. The notation $\theta <111>$ corresponds to the B^1 orientation rotated at an angle θ around the $<111>$-axes. The value of θ is approximately 15 deg. The figure is based on measurements in the vicinity of 20 subgrains of the Bs orientation for each deformation condition.

3. *Evolution of recrystallization microstructure and texture*

The main objective of the macrotexture measurements of the fully transformed material was to investigate the effect of strain on the texture development during annealing. At the lowest Zener–Hollomon parameters, the grain size is relatively large, and the statistics for the texture measurements becomes poorer; the present description is hence restricted to Zener–Hollomon parameters including and above $Z = 7 \cdot 10^{11}$ s^{-1}.

Figure 3 shows the development of recrystallization texture with strain at a Zener–Hollomon parameter of $7 \cdot 10^{11}$ s^{-1}. As seen in the figure, at the lowest strains, a very weak, nearly random annealing texture was observed. Increasing the strain to $\varepsilon = 3$, the texture is still weak, but small amounts of the Bs component ($\{0\bar{1}1\}\langle\bar{2}11\rangle$ and $\{01\bar{1}\}\langle 2\bar{1}\bar{1}\rangle$ is now observed. The Bs component is 30 deg $<111>$ oriented with respect to the B^1 component ($\{\bar{1}12\}\langle 110\rangle$ and $\{1\bar{1}\bar{2}\}\langle\bar{1}\bar{1}0\rangle$ found in the as-deformed material. At a prior strain of $\varepsilon = 5$, the Bs component is clearly visible, and at increasing strains, it continues increasing.

Table III. The Number of Potential New Grains of the Bs Orientation and Other Orientations for a Selection of Deformation Conditions; the Data Have Been Collected OIM in Partly Recrystallized Material; the Specimens Were Annealed for 5 Seconds at 480 °C

Z (s^{-1})	Strain	Bs	Other
$7 \cdot 10^{11}$	1	10 (15 pct)	57 (85 pct)
	3	47 (23 pct)	157 (77 pct)
	5	113 (41 pct)	166 (59 pct)

The recrystallized grain size was measured by using optical microscopy, and the results are displayed in Figure 4. The values in the figure are based on measurements of typically 300 to 400 grains; however, at the lowest Z value, the grain size was quite large and the measurement is based on fewer grains. The grain sizes decrease with increasing Zener–Hollomon parameter and stored energy, as expected.

The effect of strain on the recrystallized grain size was also investigated. The results are shown in Figure 5. All specimens contained close to equiaxed grains, which indicates that small particles have not interfered with the recrystallization process. As expected, the grain sizes increase with decreasing Z. Variation of the strain, however, gives a rather surprising result. As can be seen from Figure 5, the grain size at the lowest Zener–Hollomon parameters increases with increasing deformation. At a Zener–Hollomon parameter of $1 \cdot 10^{12}$ s^{-1}, the recrystallized grain size decreases up to a strain of 3, then at a strain of 3 to 10, it starts increasing. At a Zener–Hollomon parameter of $2 \cdot 10^{14}$ s^{-1}, the grain size is uniformly decreasing with strain.

IV. DISCUSSION

A. *Recrystallization of plane strain compressed material*

Nes and co-workers[1–4,9,10] found that the recrystallization process in AlMgMn-alloys is well described by including three different types of nucleation sites: (1) deformation zones around large second-phase particles, (2) cube bands, and (3) grain-boundary regions. Such a combination of nuclei was found to result in a recrystallization texture containing the Cube component and grains of random orientation. Similar results were found in the present material, and the present work will draw on the previously obtained results. A model for describing recrystallization after hot plane strain compression has been developed,[1–4] and the basic assumptions of the model are listed as follows.

1. Steady state has been reached in the investigated specimens. For the specimens deformed in the present investigation, this is assumed to be the case ($Z < 1 \cdot 10^{12}$ s^{-1} and strains >0.4).

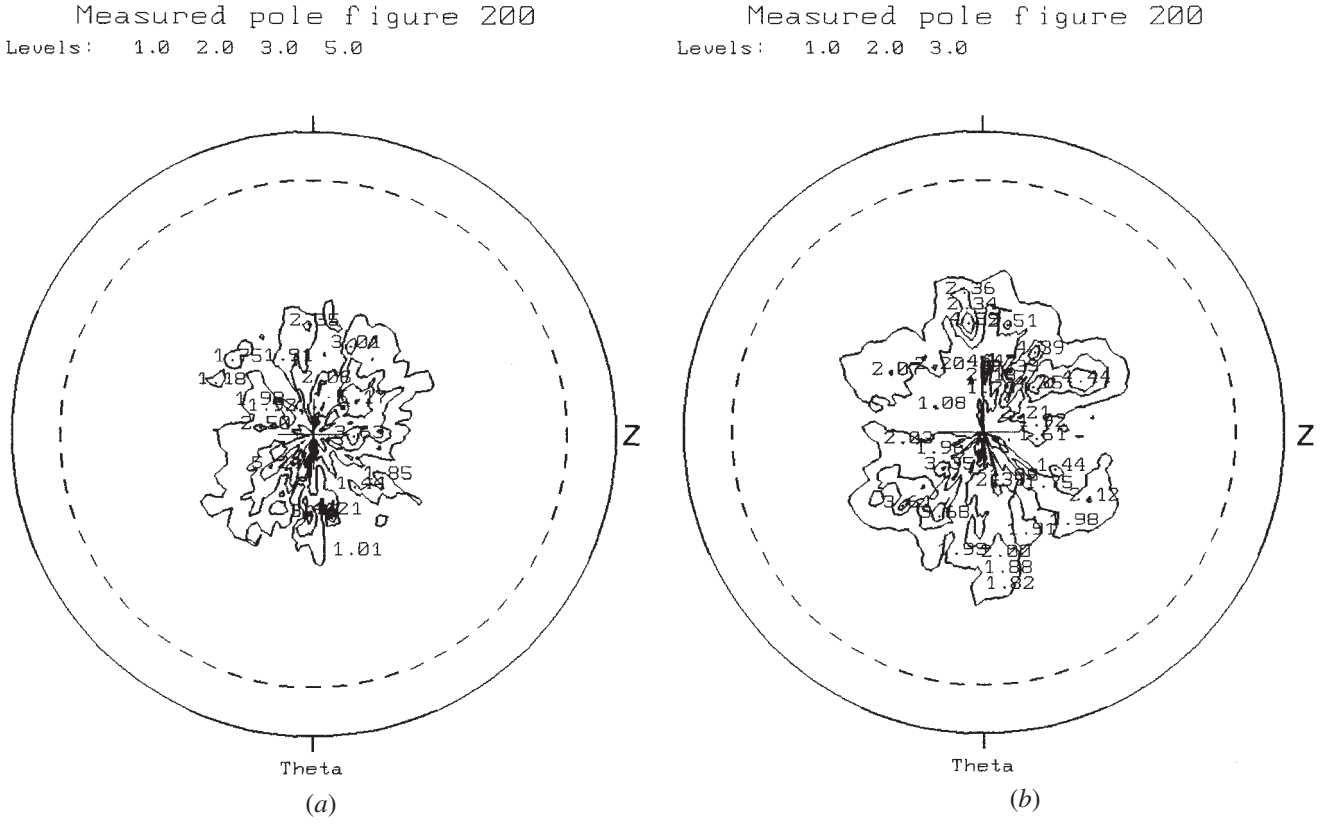

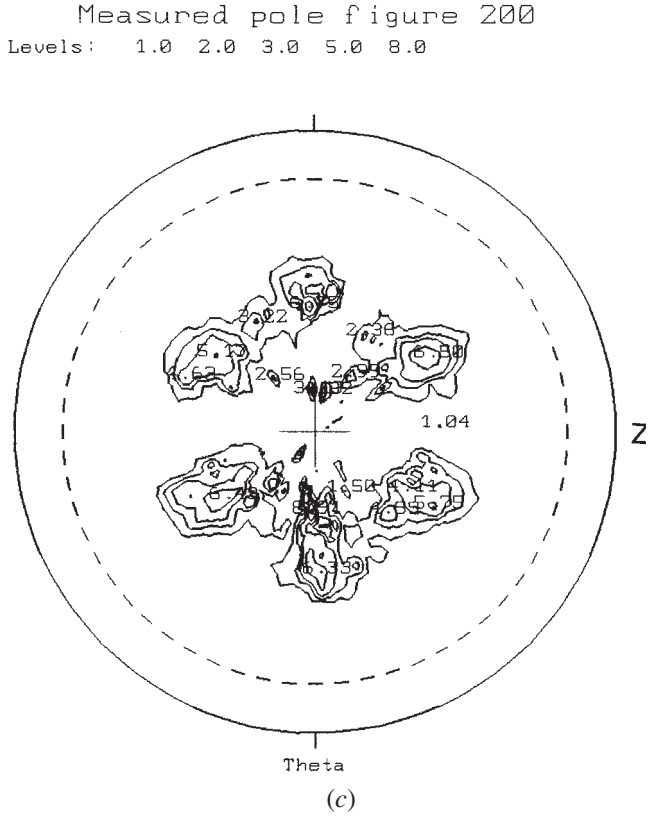

Fig. 3—Development of annealing textures with increasing prior strain illustrated by experimental {200} polefigures. All specimens have been deformed in torsion at a Zener–Hollomon parameter of $Z = 7 \cdot 10^{11}$/s and subsequently annealed at 480 °C for 21 seconds. The specimens have been deformed to different strains: (*a*) $\varepsilon = 2$, (*b*) $\varepsilon = 3$, (*c*) $\varepsilon = 5$

2. Near site saturation nucleation kinetics applies.
3. The nucleation sites are randomly distributed in space.
4. The recrystallization texture is a result of oriented nucleation.

Items (2) through (4) have been experimentally confirmed for a 3004 alloy deformed in plane strain compression,[1–4,9,10] and they are assumed to apply for the material in the present investigation as well. The calculation of the densities of nuclei from the three categories listed previously will be described in the following.

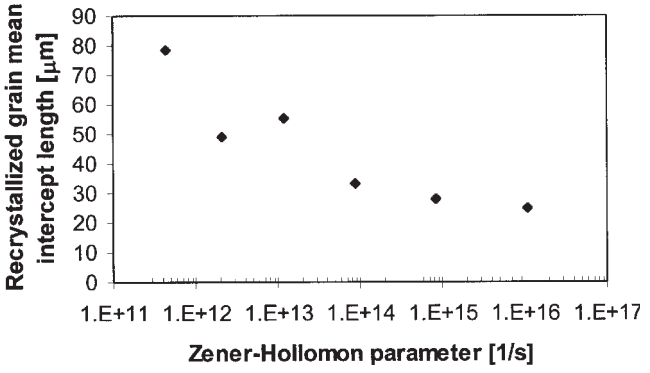

Fig. 4—Recrystallized grain sizes (given as intercept lengths) as measured by optical microscopy for a wide spectre in Z values. The Al experiments were carried out to a strain of 1.1. The material presented in this figure has been slowly cooled after homogenization.

1. *Deformation zones around second-phase particles*

Particle-stimulated nucleation is known to be an important nucleation mechanism in many commercial aluminum alloys, *e.g.*, Humphreys and Hatherly.[5] For the nucleation to occur, the particle has to be larger than a critical size, determined by the stored energy in the material; that is, $\eta_c = 4\gamma_{GB}/3P_D$, where γ_{GB} is the grain-boundary energy and P_D is the stored energy in the matrix. The density of PSN sites is determined by the particle size distribution, which is characterized through the distribution parameters N_0 and B. The following expression for the density of particle stimulated nuclei is found:

$$N_{\text{PSN}} = C_{\text{PSN}} N_0 \exp\left(-\frac{4B\gamma_{GB}}{3P_D}\right) \qquad [3]$$

where C_{PSN} is a tuning constant.

2. *Cube sites*

Thorough investigations of the nucleation at Cube bands have been carried out by Nes and co-workers.[1–4,9,10] They demonstrated that the nucleation of Cube grains is associated with Cube grains that were present in the starting material, and which remained orientation stable during deformation. The basis of the nucleation mechanism for Cube grains suggested by Vatne *et al.*[1–4] can be summarized as follows. (1) "Old"

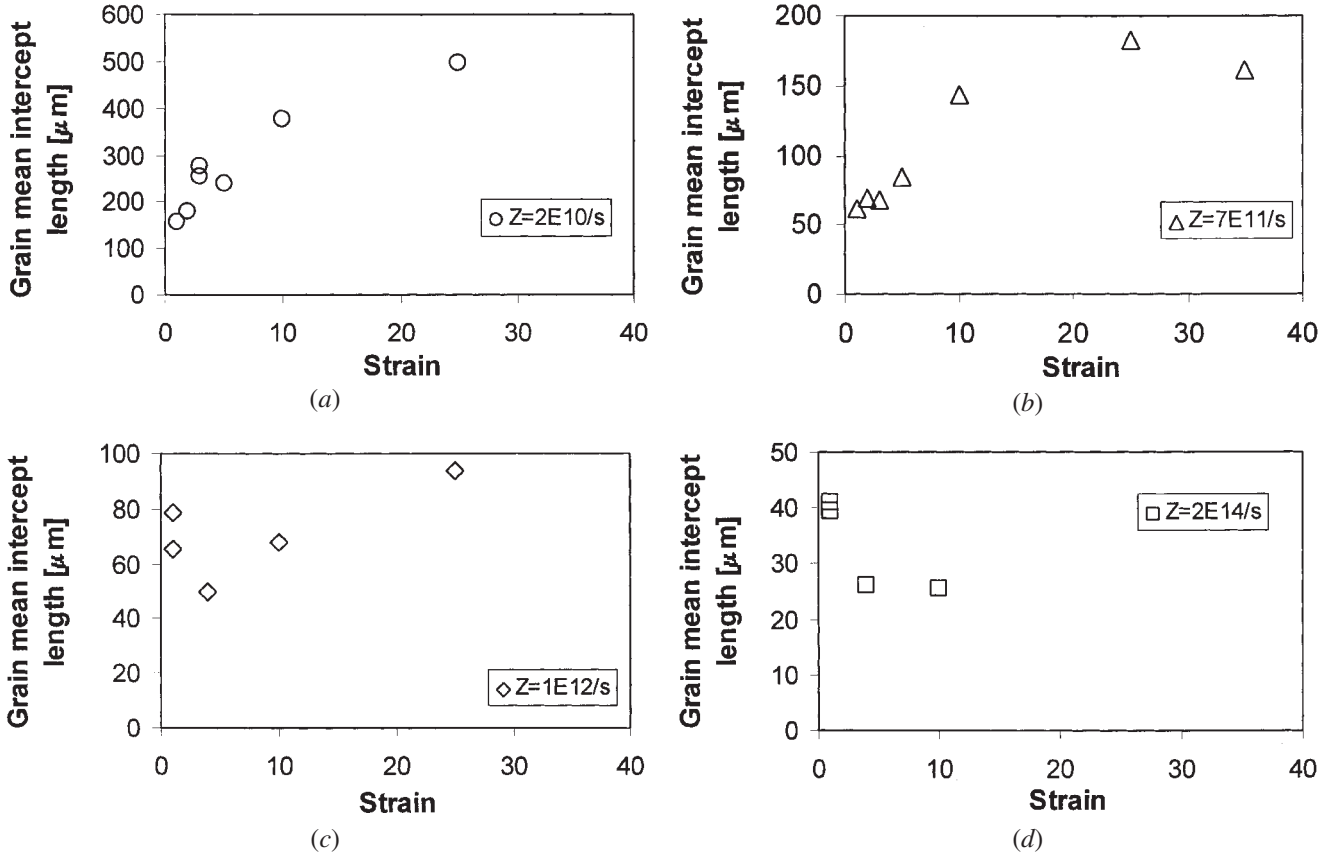

Fig. 5—Recrystallized grain mean intercept length as a function of strain for four different Zener–Hollomon parameters. The grain size measurements are performed by optical intercept scans, and the plotted values are a weighted mean between the θ and z directions: (*a*) $Z = 2{\cdot}10^{10}$/s (T = 523 °C, strain rate = 1.3/s) annealed at 523 °C; (*b*) $Z = 7{\cdot}10^{11}$/s (T = 486 °C, strain rate = 13/s) annealed at 486 °C; (*c*) $Z = 1{\cdot}10^{12}$/s (T = 404 °C, strain rate = 1.2) annealed at 500 °C; and (*d*) $Z = 2{\cdot}10^{14}$/s (T = 304 °C, strain rate = 1.2/s) annealed at 500 °C. The material was quenched after deformation.

Cube grains remain metastable during deformation and are deformed to bandlike shapes. (2) Subgrains within the Cube bands have a size advantage compared to the subgrains of other orientations. The typical size distribution of the Cube subgrains was found to have a long tail of large subgrains. (3) The existence of Cube-S high-angle boundary promoted nucleation from Cube bands. The density of Cube sites was found to be

$$N_C = \frac{2C_C\bar{\delta}_C R_C(1 - R_C)R_S S_C^*}{D_0}[\exp(\varepsilon) + \exp(-\varepsilon) + 1] \quad [4]$$

where C_C is a modeling parameter, $\bar{\delta}_C$ is the average size of the Cube subgrains, R_C is the instantaneous volume fraction of Cube in the material, R_S is the volume fraction of S in the material, S_C^* is the number of subgrains per unit volume larger than the critical subgrain size, D_0 is the average size of the Cube grains in the starting material, and ε is the strain.

3. *Grain-boundary regions*

Nucleation at pre-existing high-angle boundaries has been included basically to account for the large fraction of random oriented grains seen in the recrystallized material even in specimens deformed at low Z values. In addition, nucleation at grain-boundary regions is often found to be responsible for a retained recrystallization texture. The following expression for the density of grains originating from the grain-boundary regions has been found.[1–4]

$$N_{GB} = \frac{2C_{GB}\bar{\delta}_C(1 - R_C)\,S_{GB}^*}{D_0}[\exp(\varepsilon) + \exp(-\varepsilon) + 1] \quad [5]$$

where C_{GB} is a modeling parameter, $\bar{\delta}$ is the average subgrain size, and S_{GB}^* is the density of overcritical nuclei in the grain-boundary zones.

4. *Stored energy*

When calculating the number of nuclei, the driving pressure for recrystallization is an essential parameter. The following expression for the driving pressure is commonly used:

$$P_D = \Gamma\rho_i + \frac{3\gamma_{SB}}{\bar{\delta}} \quad [6]$$

where γ_{SB} is the subgrain boundary energy, $\bar{\delta}$ is the mean subgrain size $\Gamma = Gb^2/2$ is the dislocation line tension, and ρ_i is the dislocation density in the interior of the subgrains.

When the density of nucleation sites has been calculated, assuming that the recrystallization texture is a result of oriented nucleation, the resulting recrystallization texture is found. In addition, the resulting grain size is easily found from the total density of nucleation sites, $N_{TOT} = N_{PSN} + N_C + N_{GB}$:

$$D = \sqrt[3]{\frac{1}{N_{TOT}}} \quad [7]$$

5. *Model predictions*

The model described previously in Chapter IV A, Section 1-4, will now be compared to the experimental results. Figures 6(a) and (b) show the predicted values together with the experimental findings in the present investigation, supplemented with some values obtained from the literature. As can be seen from the figures, the model has good predictive capabilities. The volume fraction of Cube is seen to decrease as a function of the Zener– Hollomon parameter. This is due to the decrease in the fraction of Cube in the as-deformed material. With an increasing Zener–Hollomon parameter, the old Cube grains in the as-deformed material are believed to gradually rotate into other orientations, and the fraction of Cube nucleation sites hence decreases. The result is an increasing fraction of nucleation sites with the random orientation. The model predicts that at low Zener–Hollomon parameters, the fraction of PSN sites is negligible, while when increasing the Zener–Hollomon parameter, the fraction of PSN sites increases at the same time as the fraction of sites originating from the grain boundaries starts to decrease. Increasing the Zener–Hollomon parameter, the particle-stimulated nucleation increases and can eventually be the dominating mechanism.

The recrystallized grain size is seen to decrease with increasing strain. This is due to an increasing number of nuclei of the Cube-type and the grain-boundary type. The number of particle-stimulated nuclei is, according to the preceding assumptions, not expected to change with strain. Hence, the volume fraction of the grains originating from large particles is assumed to decrease with strain. Since the volume fraction of Cube grains increases with strain, the volume fraction of grains originating from grain-boundary areas is expected to be approximately constant. However, the number of grains originating from the grain-boundary areas increases, which is due to the area of the old grain boundaries increasing with strain. In the same manner, the area of the original boundaries of the Cube grains increases with strain, which leads to an increasing fraction of Cube grains. In addition, the amount of S-oriented grains in the as-deformed material increases with strain. And if it is assumed that the Cube-S combination promotes recrystallization, this will lead to even more nuclei of the Cube orientation. In Figure 6(a), experimental measurements at strains ranging from 0.4 to 2.3 have been included, while the model is applied at a strain of 2. Hence, there is a large scatter in the experimental results and the modeled result for low Zener–Hollomon parameters. Using the model to predict the grain size at a strain of 1.7, a significantly larger grain size is found at the lowest Zener–Hollomon parameters. At $Z = 2\cdot10^{10}$ s^{-1}, a grain mean intercept length of about 210 μm is found, which still is slightly lower than the values obtained experimentally.

B. *Recrystallization of material deformed in torsion*

An interesting question now becomes; Is the PSC recrystallization model also applicable in torsion? The answer to this question is not obvious. First of all, the PSC model predicts the formation of Cube, which is not found in material deformed in torsion and subsequently recrystallized. Second, when annealing the torsion specimens, large amounts of the Brass component were found. And third, in plane strain compression, a quite steep increase in grain-boundary area is expected, compared to the corresponding increase in torsion. Based on the experimental results from the recrystallization of specimens deformed in torsion, a model for predicting the density of nuclei of recrystallization in torsion

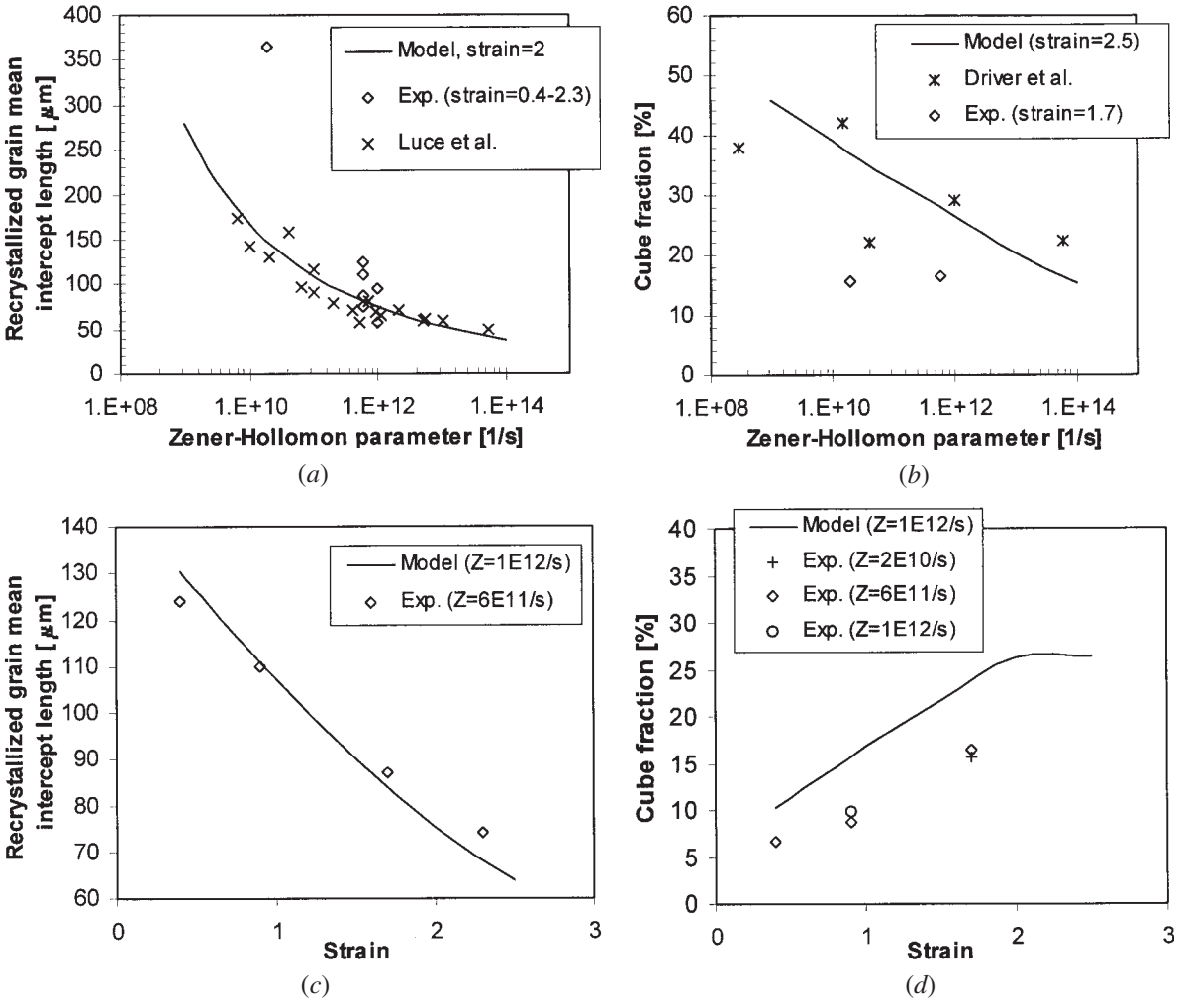

Fig. 6—Variation of grain mean intercept length and volume fraction Cube in the recrystallized material with Zener–Hollomon parameter and strain. The solid-drawn lines correspond to the model predictions and the symbols correspond to values found experimentally. The crosses in (a) are taken from the work of Luce and Brandt,[14] while the crosses in (b) are taken from the work of Fillit *et al.*[15]

will now be presented. The model is based on the previously described model for PSC (Vatne *et al.*[1–4]).

It has been assumed that the nucleation of recrystallization is fully described by four types of nuclei: nucleation at Bs-oriented bands originating from Bs-oriented grains in the starting material, nucleation of Bs-oriented grains from small areas of the Bs orientation formed during deformation, nucleation at large second-phase particles, and nucleation of random oriented grains at old grain boundaries.

1. *Nucleation of grains of the Bs orientation*

The Bs grains originate from the boundary regions of the original Bs grains and the boundary regions of B^1-oriented bands formed during deformation. In both cases, the formation of nuclei is dependent on the available grain-boundary area of the orientations in question. An expression for the density of nuclei of the Bs orientation originating from the Bs bands can be given by the following relationship, originally proposed in a slightly different form by Vatne *et al.*[1–4] to account for the nucleation of grains of the Cube orientation in plane strain compressed material:

$$N_{\mathrm{Bs}}^{0} = C_{\mathrm{Bs}}^{0}\,\bar{\delta}_{\mathrm{Bs}}\,A_{\mathrm{Bs}}(\varepsilon)(1 - R_{\mathrm{Bs}}^{0})S_{\mathrm{Bs}}^{*} \qquad [8]$$

where C_{Bs}^{0} is a modeling constant, $\bar{\delta}_{\mathrm{Bs}}$ is the average subgrain size of the Bs-oriented subgrains, $A_{\mathrm{Bs}}(\varepsilon)$ is the surface area per unit volume of Bs-oriented bands, R_{Bs}^{0} is the fraction of grains of the Bs orientation, and S_{Bs}^{*} is the density of subgrains of the Bs orientation larger than the critical size required for nucleation of recrystallization.

The Bs-oriented nuclei originating from the boundary regions of the B^1-oriented grains will depend on the surface area per unit volume of the B^1-oriented material, $A_{\mathrm{B}}(\varepsilon)$. As already discussed, the volume fraction of the B^1 component increases with strain, and the nucleation expected from grains of the Bs orientation formed during deformation will hence also change with strain. An expression for the nucleation of recrystallized grains from the Bs-oriented areas formed during deformation can be stated as follows:

$$N_{\mathrm{Bs}}^{T} = C_{\mathrm{Bs}}^{T}\,\bar{\delta}_{\mathrm{Bs}}\,A_{\mathrm{B}}(\varepsilon)(1 - R_{\mathrm{Bs}}^{0})\,k_{\mathrm{Bs}}(\varepsilon)\,S_{\mathrm{Bs}}^{*} \qquad [9]$$

where C_{Bs}^{T} is a modeling constant and $k_{\mathrm{Bs}}(\varepsilon)$ is the fraction of the outer part of the B^1-oriented bands that rotate into the Bs orientation.

Using simple geometry,[14] considering the deformation of an original cubic grain with edge length equal to the

average original grain size D_0, deformed to a strain of ε, the surface area per unit volume of the original grains is easily seen to be given by the following expression:

$$A_{Bs/B}(\varepsilon) = \frac{2R_{Bs/B}}{D_0}\left[\sqrt{1 + 3\varepsilon^2} + \frac{1}{\sqrt{1 + 3\varepsilon^2}} + 1\right] \quad [10]$$

where $R_{Bs/B}$ is the volume fraction of grains of the Bs or the B^1 orientation.

From the preceding considerations, the expression for the density of nucleation sites of the Bs orientation becomes:

$$N_{Bs} = C_{Bs}\bar{\delta}_{Bs}(1 - R^0_{Bs})S^*_{Bs}\frac{2}{D_0}\left[\sqrt{1 + 3\varepsilon^2} + \frac{1}{\sqrt{1 + 3\varepsilon^2}} + 1\right] \cdot [R^0_{Bs} + R_B(\varepsilon)\, k_{Bs}(\varepsilon)] \quad [11]$$

The parameter C_{Bs} is introduced as a tuning constant, and gives information on the strength of the mechanism of nucleation at Bs grains. Expression [11] is valid only for "small" strains, that is, strains smaller than about 3 to 5. Above this strain, the expression for the grain-boundary area is no longer valid, and other considerations are required.

2. *Nucleation at deformation zones developed around second-phase particles*

The calculation of the density of sites nucleated at second-phase particles has been outlined in Section A, and the density of the PSN sites is given by Eq. [3].

3. *Nucleation at old grain boundaries*

The expression used for the nucleation at prior grain boundaries is similar to the corresponding expression in plane strain compression. The difference in the two expressions originates in the difference in the change in grain-boundary area.

$$N_{GB} = C_{GB}\frac{2\bar{\delta}\cdot S^*_{GB}}{D_0}\left[\sqrt{1 + 3\varepsilon^2} + \frac{1}{\sqrt{1 + 3\varepsilon^2}} + 1\right] \quad [12]$$

where the symbols in the equation are as previously defined. The constant C_{GB} is introduced as a modeling constant.

4. *Predictions of the model compared to experimental data*

The model described above will now be applied to predict the change in nucleation density and recrystallized grain size with the changing deformation conditions. At low strains, the number of outgrown grains is expected to be negligible, and accordingly, the model has been used to predict the change in recrystallized grain size with the Zener– Hollomon parameter for low strains. The results are displayed in Figure 7. As can be seen from the figure, the recrystallized grain size decreases with an increasing Zener– Hollomon parameter. This is as expected since the number of nuclei rises with increasing Zener–Hollomon parameter and increasing stored energy.

An example of the development in recrystallized grain size with strain is shown in Figure 8, showing the change in recrystallized grain size at $Z = 7\cdot10^{11}\ s^{-1}$. The experimental "grain sizes" have been calculated from partly recrystallized

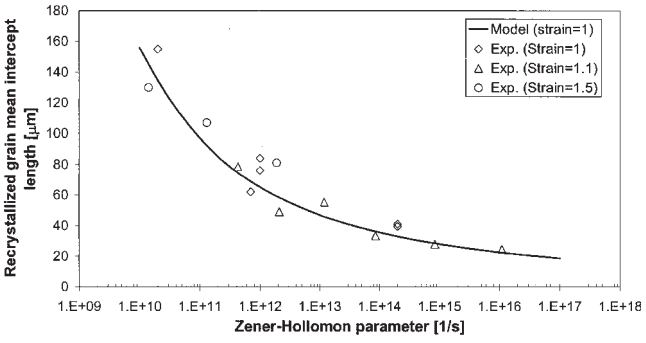

Fig. 7—Comparison between the model predictions and the experimentally obtained values for the recrystallized grain mean intercept lengths at small strains. The material deformed to a strain of 1 and to Zener–Hollomon parameters less than $7\cdot10^{11}$/s has been quenched after homogenization, while the rest has been either slowly cooled (strain of 1) or industrially homogenized (strains of 1.1 and 1.5). The results at a strain of 1.5 are taken from the work of Nord-Varhaug.[16]

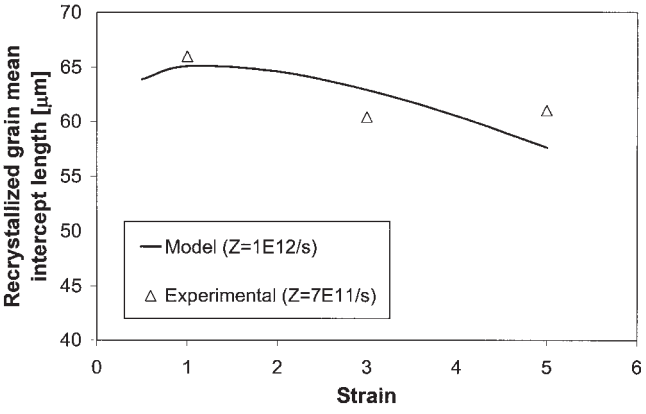

Fig. 8—Change in recrystallized grain mean intercept length with strain, as predicted from the model and as measured from experiments. The experimental data have been obtained by counting the number of potential new grains of recrystallization at a certain area, and subsequently estimating the diameter of the fully recrystalized grains.

specimens by measuring the density of potential new grains. When modeling this particular case, it was taken into account that the subgrain size and, accordingly, the driving pressure of recrystallization were found to change with strain. The increase in stored energy at increasing strains led to a less pronounced fall in grain size. The change in grain size with strain at other Z values was found to be similar. The decrease in the predicted size of the recrystallized grains is essentially due to an increase in the number of Bs-oriented nuclei with strain. The increase in the area of the original grains with strain leads to an increasing volume fraction of nuclei with Bs orientation. However, the main reason for the increase in the number of nuclei is the formation of B^1-oriented grains, which small volumes of Bs-oriented grains have been observed to form from.

By comparing the partly recrystallized and the fully recrystallized specimens at large strains, it is obvious that some of the nuclei/grains have to be consumed during the annealing process. The consumption of the disappearing grains may occur either in the partly or fully transformed material. The requirement being only that two or more of the nuclei or transformed grains are replaced by one grain. The

most probable course of events, suggested by the experimental observations, is that a large grain grows into a single transformed grain or a group of grains.

At large strains ($\varepsilon > 5$), the nucleation mechanisms studied previously are not expected to prevail. The modest activity of the large particles as nucleation sites is expected to become even weaker due to the increasing particle breakup at increasing strains. In addition, the microstructure changes, resulting in a break up of the elongated bands, and hence nucleation at prior grain boundaries is not expected. The recrystallization texture at high strains still consists of the Bs component in addition to grains of random orientation. However, the Bs component is now totally dominating, indicating that nuclei of random orientation are either not formed, or are "out-grown" by the grains of the Bs orientation. At large strains, island regions of the Bs orientation and the random orientation are found. In general, provided that they have a size advantage, these island subgrains make ideal nucleation sites. In the deformed material, it was found that the density of subgrains of the Bs orientation remained approximately constant, while the density of subgrains of the random orientation decreased with strain. Hence, there seems to be a decrease in potential nuclei with strain, explaining the recrystallized grain size with strain.

If it is assumed that each subgrain of the Bs and the random orientation constitute a viable nuclei of recrystallization, the resulting grain size can be estimated from the as-deformed material. The difference in the recrystallized grain size predicted from the partly recrystallized specimens and that measured from the fully recrystallized specimens has been found to be larger at the largest strain. This indicates that an increasing fraction of nuclei are "outgrown" at increasing strains.

In summary, the reason for the increasing grain size with strain seems to be twofold. (1) The total number of nuclei decreases with strain, due to a decrease in the number of random oriented island regions. (2) The number of small grains consumed by other grains seems to be larger at higher strains.

V. CONCLUSIONS

1. At small strains, regions of the Bs orientation ({110}<112>) in the as-deformed material are present as elongated bands and small regions containing one subgrain or a small group of subgrains.
2. The Bs orientation ({110}<112>) seems to form during deformation in torsion by a 30 deg <111> rotation of small regions in the boundary region of the B-oriented ({112}<110>) bands.
3. Some of the nuclei that are starting to grow are outgrown during the recrystallization process. The number of outgrown nuclei increases with strain at large strains.
4. Based on the experimental investigation, a model describing the change of nucleation sites with strain and Zener–Hollomon parameter during torsion has been developed. This model has been compared to a similar model that was previously developed and predicts the development of recrystallized grain size and texture with strain and the Zener–Hollomon parameter in plane strain compression. The model developed for torsion predicts a relatively slow increase in the density of nuclei with increasing strain compared to the plane strain compression model. The development with the Zener–Hollomon parameters for the two models is similar.

ACKNOWLEDGMENTS

Thanks are due to Hydro Aluminium for financial support, and for providing the material. The present work has benefited from a major European Community programme: the Brite-Euram project REAP, Project No. BE96-3364.

REFERENCES

1. H.E. Vatne, T. Furu, R. Ørsund, and E. Nes: *Acta Metall.*, 1996, vol. 44, p. 4463.
2. H.E. Vatne, K. Marthinsen, R. Ørsund, and E. Nes: *Metall. Mater. Trans. A*, 1996, vol. A27, pp. 4133-44.
3. H.E. Vatne, T. Furu, and E. Nes: *Mater. Sci. Technol.*, 1996, vol. 12, pp. 201-10.
4. H.E. Vatne, R. Shahani, and E. Nes: *Acta Metall. Mater.*, 1996, vol. 44, pp. 4447-61.
5. F.J. Humphreys and M. Hatherly: *Recrystallization and Related Annealing Phenomena*, Pergamon Press, Oxford, United Kingdom, 1995.
6. P.A. Hollonshead and T. Sheppard: in *Aluminium Technology*, The Institute of Metals, London, 1986, vol. 317, pp. 73.1-73.10.
7. J. Hirsch: *Mater. Sci. Technol.*, 1990, vol. 6, pp. 1048-57.
8. H. Weiland and J. Hirsch: *Textures & Microstr.*, 1990, vols. 14-18, p. 647.
9. O. Daaland and E. Nes: *Acta Mater.*, 1996, vol. 44 (4), pp. 1389-1411.
10. O. Daaland and E. Nes: *Acta Mater.*, 1996, vol. 44 (4), pp. 1413-35.
11. T. Pettersen, B. Holmedal, and E. Nes: *Metall. Mater. Trans. A*, 2003, vol. 34A, pp. 2737-44.
12. N.J. Silk and M.R. van der Winden: *Mater. Sci. Technol.*, 1999, vol. 15, p. 295.
13. T. Pettersen and E. Nes: *Metall. Mater. Trans. A*, 2003, vol. 34A, pp. 2727-36.
14. R. Luce and A. Brandt: IBF, RWTH, Aachen, personal comunication, 1998.
15. R. Fillit, F. Perocheau, and J. Driver: EU Project No. REAP.3.1, EMSE, Saint Etienne, France, Report No. 98002, 1998.
16. K. Nord-Varhaug: personal communication, Norwegian University of Science and Technology, NTNO, Trondheim, Norway, 1998.